

Elastic Depth Profiling of Soft Tissue by Holographic Imaging of Surface Acoustic Waves

Karan D. Mohan^a, William W. Sanders^a, Amy L. Oldenburg^{a,b}

^aUniversity of North Carolina at Chapel Hill, Department of Physics and Astronomy, Chapel Hill, NC, USA

^bUniversity of North Carolina at Chapel Hill, Biomedical Research Imaging Center, Chapel Hill, NC, USA

aold@physics.unc.edu

Abstract: Digital holography is used to image surface acoustic waves in tissue-mimicking silicone phantoms. Elastic depth profiles, at depths up to 30mm, are then obtained from the phase velocity dispersion curves by solving the inverse problem.

OCIS codes: (090.1995) Digital Holography; (170.3880) Medical and biological imaging.

1. Introduction

Elastography is a promising method for the early detection of breast cancer, since tumors exhibit an elastic modulus 3-10× greater than healthy tissue [1]. Several imaging modalities have thus been developed that contrast soft-tissue elasticity [2, 3]. We recently reported a new elastography technique based on digital holography [4], which is advantageous as it provides the ability to image a wide area along with nanometer displacement sensitivity. In this paper, we use image plane digital holography to map surface acoustic waves (SAWs) on silicone phantoms that are mechanically similar to breast tissue. The phantoms' elastic properties are then inferred from the SAW velocities. This method is similar to techniques used in non-destructive testing for materials analysis, where the internal stiffness properties are inferred from SAW behavior [5]. In fact, soft tissue elastography from SAWs is a growing area of interest [6, 7] – many of these experiments, however, have been accomplished using Doppler vibrometry, which is unable to rapidly analyze an entire surface region.

As a first step toward 3D elastography imaging, here we investigate 1D (depth-dependent) elastography. Since the penetration depth of SAWs (in particular Rayleigh Waves) is approximately one wavelength, variations in elasticity as a function of depth are observed as variations in SAW velocity versus wavelength. Thus, in a phantom composed of multiple layers of varying elastic moduli, SAWs at a lower frequency (longer wavelength) exhibit velocities corresponding to the elastic modulus of the lower layers, and vice versa. Here we present, for the first time, an inversion algorithm based on this theoretical relationship that is applied to the holographically measured dispersion curves, yielding the elasticity vs. depth profile in single- and multi-layered phantoms.

2. Methods

2.1 Experimental Setup

The in-line, image plane, digital holography system employed to map SAWs is illustrated in Fig. 1(a). The beam from a 5mW, 633nm Helium-Neon laser (Thorlabs, Newton, NJ) is divided into reference and object paths with a 92:8 beamsplitter (with 92% of the power going along the object path). A 2.5× beam expander, in conjunction with a 2" diameter downward reflecting mirror, was then used to illuminate the phantom sample. The diffusely reflected light (speckle) from the phantom was then directed through a 200mm focal length, 2-in diameter imaging lens, onto the sensor of a high-speed CMOS camera (Photron FastCam SA3, Japan). A 1:1 magnification was used, mapping an 8.5mm x 8.5mm area of the phantom onto 512 × 512 pixels of the camera array. An adjustable aperture was utilized behind the imaging lens, so that the speckles were resolvable by the camera sensor. The camera framerate was set at 3000Hz, ensuring ≥10× sampling of each period of the SAWs.

Light along the reference path was passed through a spatial filter and 15× beam expander before being directed onto the camera. The speckled image of the phantom interacts with this reference beam, forming an interferogram on the camera. A neutral density filter was placed along the reference arm to optimize the interference signal within the dynamic range of the camera. As SAWs propagate along the surface of the phantom, a phase shift is induced in the interferogram caused by the changing optical path difference between the reference and scattered fields. The system is therefore sensitive to out-of-plane surface displacements.

A piezo-electric transducer (Kinetic Ceramics, Hayward, CA), placed immediately outside the illumination area, was used to excite the surface waves. The transducer was driven at various frequencies between 70-320Hz. The mechanical waves were allowed to reach a steady state at each frequency, before the camera recorded the interferogram in real time. A temporal phase shifting algorithm, detailed in Ref [4], is then used to obtain a map of the *phase of the SAW* (not to be confused with the optical phase, which is used to infer the SAW phase). The speed of the SAWs is then obtained by inspecting the time series of phase maps (illustrated in Figs. 1(b) and (c)).

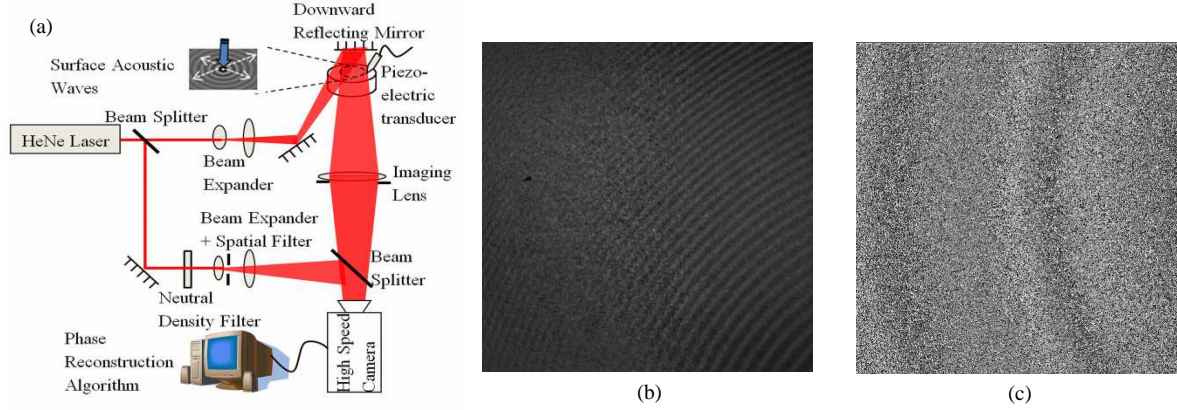


Fig. 1 (a) Experimental Setup (b) Example of interferogram and (c) the corresponding phase reconstruction.

2.2 Inversion of Dispersion Data

The behavior of Rayleigh waves propagating in elastically homogeneous media is well known, with a phase velocity (independent of frequency) given approximately by:

$$c_R \approx (0.87 + 1.12\nu)/(1 + \nu) \sqrt{E/2\rho(1 + \nu)} \quad (1)$$

where E is the Young's modulus, ρ is the density and ν is the Poisson's ratio of the material [8]. The SAW velocity in heterogeneous samples where the elastic properties vary with depth is frequency-dependent. An approach to determining the SAW speed in this situation is to divide the sample into a large number of homogeneous layers. Wave equations are then written for each layer, along with the conditions of continuity across boundaries between the layers, a free top surface and finiteness at infinity. This results in a system of $4N$ equations (where N is the number of layers), and the determinant of this system contains an implicit relationship between the phase velocity and frequency [9]. This approach, while accurate, requires tedious numerical computation which is not easily amenable to an inverse process for determining the elastic properties in each layer.

Our approach is to recognize that the amplitude of Rayleigh waves are exponentially decaying in depth [8, 9], and to approximate the effective Young's modulus "felt" by the SAW as the average of the elasticities of the individual layers, weighted by the SAW amplitude at each depth, as follows:

$$E_{\text{eff}}(f) = \int_0^L \left(\alpha e^{-2\pi\alpha(f/c_R)y} - \frac{\beta^2 + 1}{2\beta} e^{-2\pi\beta(f/c_R)y} \right) E(y) dy \bigg/ \int_0^L \left(\alpha e^{-2\pi\alpha(f/c_R)y} - \frac{\beta^2 + 1}{2\beta} e^{-2\pi\beta(f/c_R)y} \right) dy \quad (2)$$

where $E(y)$ is the Young's modulus as a function of depth y , f is the SAW frequency, L is the total depth of the sample, and α and β are constants that depend on Poisson's ratio [8]. Equation (2) may then be solved together with equation (1) to obtain a dispersion curve $c_R(f)$ for a given $E(y)$ (Note that $E_{\text{eff}}(f)$ depends on the phase velocity c_R , so this system must thus be solved iteratively). While this forward model is *ad hoc*, we find that the dispersion curves obtained are close to those calculated by the more accurate determinant based method, within the experimental error.

Using this integral model, we may now solve the linear inverse problem of determining $E(y)$ from an experimentally measured dispersion curve, $c_R(f)$. Using the layers model, we begin by discretizing the integral (2) into a linear matrix system $AE = E_{\text{eff}}$. Here, E_{eff} is a vector of discrete points representing the measured effective elasticity at each f (obtained from measurements of $c_R(f)$ via equation (1)), A is the observation matrix computed from the integral expressions in (2), and E is a vector representing the Young's modulus at each depth, which we seek. Since inverse problems are highly sensitive to small errors, we used Total Variation regularization [10], in which we determine E by minimizing $\|AE - E_{\text{eff}}\|_2^2 + \gamma(TV(E))$, where $TV(E)$ is the Total Variation of E . γ is a parameter adjusted to scale the amount of regularization, which was chosen by the L-curve method [11].

3. Results & Discussion

Experimental results demonstrating the methods above are illustrated in Fig. 2. Two phantoms that mimic optical and mechanical breast tissue properties, prepared according to previously described methods [4], were studied. The first (Figs. 2(a) and 2(c)) was a homogeneous phantom of 30mm depth and a Young's modulus of 26.5kPa. The second sample (Figs. 2(b) and 2(d)) was composed of two layers: a 15mm soft upper layer with Young's modulus of 6.37kPa, and a 15mm stiff lower layer with a Young's modulus of 26.5kPa. Figs. 2(a) and 2(b) compare the experimental dispersion behavior with theoretical curves determined from our forward model in Eq. (2).

As shown in Fig. 2(a), the homogeneous phantom shows little to no dispersion, as expected. On the other hand, the heterogeneous sample shows a negative dispersion (Fig 2(b)), which matches well with the expected behavior. The corresponding elastic profiles obtained by solving the inverse problem are illustrated in Figs. 2(c) and 2(d), along with the independently calibrated values for the two phantoms. The results indicate good agreement between the results of the inversion and the true elasticity distributions, within an experimental uncertainty of $\sim 10\%$.

These results demonstrate the potential application of digital holography for elastography of soft tissues at clinically useful depths (30mm). Further work is needed to reduce experimental uncertainty and to study the effect of tissue viscoelasticity on the dispersion data. Importantly, the nanoscale sensitivity of holography allows for the detection of waves generated by a very small excitation, thus making the method minimally invasive. Holographic elastography therefore provides a novel, minimally-invasive, optical sensing method for the detection of breast cancer or other diseases that cause variations in tissue elasticity from that of healthy tissue.

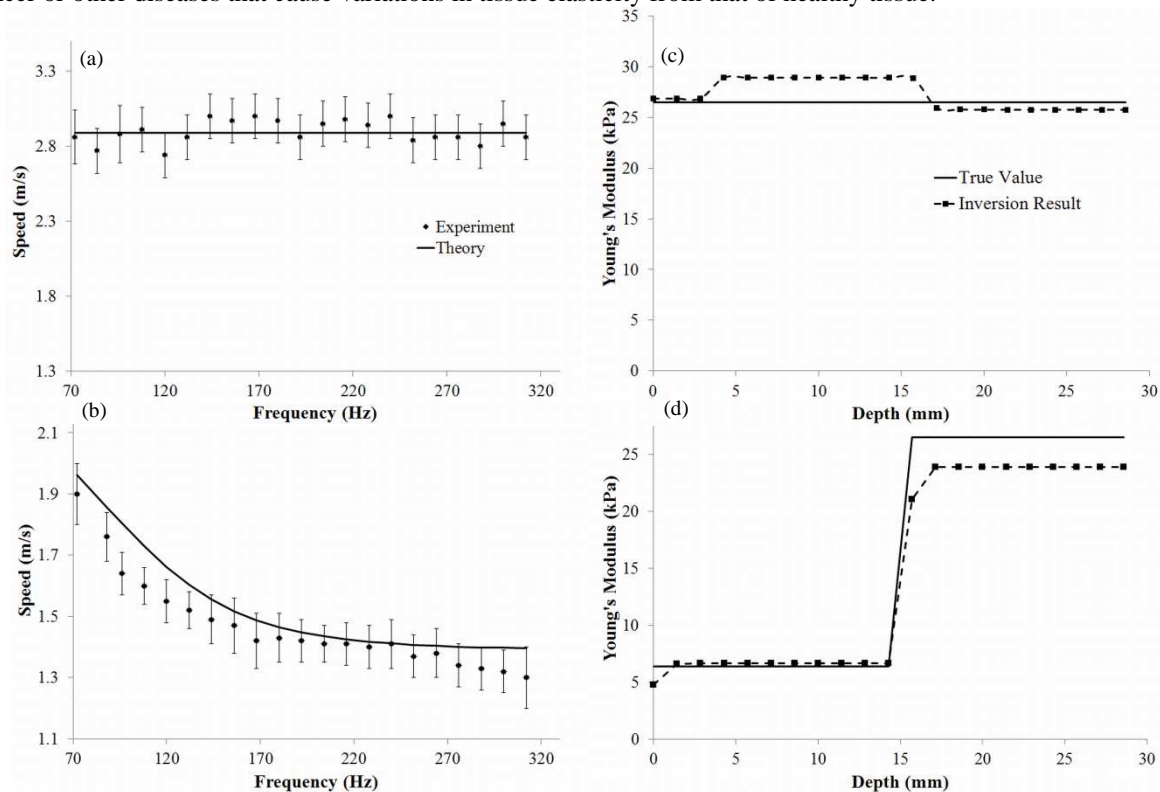


Fig. 2 SAW dispersion curves for (a) homogeneous phantom (b) 2-layer heterogeneous phantom. Also shown is the corresponding Young's modulus profile, obtained by inversion, for (c) the homogeneous phantom and (d) the heterogeneous phantom.

4. References

- [1] A. Samani, J. Zubovits, and D. Plewes, "Elastic moduli of normal and pathological human breast tissues: an inversion-technique-based investigation of 169 samples," *Phys. Med. Biol.* **52**, 1565 (2007).
- [2] J. Ophir, I. Cespedes, H. Ponnekanti, Y. Yazdj, and X. Li, "Elastography: a quantitative method for imaging the elasticity of biological tissues," *Ultrason. Imaging* **13**, 111 (1991).
- [3] D. B. Plewes, J. Bishop, A. Samani, and J. Sciarretta, "Visualization and quantification of breast cancer biomechanical properties with magnetic resonance elastography," *Phys. Med. Biol.* **45**, 1591 (2000).
- [4] S. Li, K. D. Mohan, W. W. Sanders and A. L. Oldenburg, "Toward soft-tissue elastography using digital holography to monitor surface acoustic waves", *J. Biomed. Opt.* **16**, 116005 (2011).
- [5] G. A. Gordon and B. R. Tittmann, "Surface acousticwave determination of subsurface structure," *Nondestr. Test. Eval.* **11**, 21 (1994).
- [6] X. Zhang and J. F. Greenleaf, "Estimation of tissue's elasticity with surface wave speed," *J. Acoust. Soc. Am.* **122**, 2522 (2007).
- [7] T. J. Royston, H. A. Mansy, and R. H. Sandler, "Excitation and propagation of surface waves on a viscoelastic half-space with application to medical diagnosis," *J. Acoust. Soc. Am.* **106**, 3678 (1999).
- [8] K. F. Graff, *Wave Motion in Elastic Solids*, (Dover, New York, 1991), Chap. 6.
- [9] C. Glorieux, W. Gao, S. E. Kruger, K. V. de Rostyne, W. Lauriks, and J. Thoen, "Surface acoustic wave depth profiling of elastically inhomogeneous materials," *J. Appl. Phys.* **88**, 4394 (2000).
- [10] J. Dahl, P. C. Hansen, S. H. Jensen, T. L. Jensen, "Algorithms and software for total variation image reconstruction via first-order methods," *Numer. Algor.* **53**, 67 (2010).
- [11] P. C. Hansen and D. P. O'Leary, "The Use of the L-Curve in the Regularization of Discrete Ill-Posed Problems," *SIAM J. Sci. Comput.*, **14**, 1487 (1993).